Kinetics and Thermodynamics Study of Ammonia Leaching on Spent LMR-NMC Battery Cathodes

Indra Perdana*, Muhammad Irfan Rahman, Doni Riski Aprilianto, Himawan Tri Bayu Murti Petrus, and Divita Hayyu Kinanti

Sustainable Mineral Processing Research Group, Department of Chemical Engineering, Faculty of Engineering, Universitas Gadjah Mada, Jl. Grafika No. 2, Yogyakarta 55281, Indonesia

*** Corresponding author:**

email: iperdana@ugm.ac.id

Received: January 19, 2024
Accepted: March 19, 2024

DOI: 10.22146/ijc.93312

Abstract: *The recycling of spent lithium NMC-type batteries, widely used in electric vehicles, presents a challenge due to manganese content, which complicates metal separation and purification. This study explored a selective leaching process using ammonia to recover metals from high-manganese-content LMR-NMC cathodes. By adjusting the $(NH_4)_2SO_4$ reagent concentration to 1–2 M and maintaining the temperature between 50–80 °C, the recovery rates of lithium, nickel and cobalt metals were enhanced, leaving manganese primarily as residue in the form of $Mn(OH)_2$ and $(NH_4)_2Mn(SO_4)_2$. A kinetics model, integrating an equilibrium-shrinking core model with a modified temperature-dependent Arrhenius approach, accurately simulates the metal recovery. The activation energies of the forward leaching reactions of Li, Ni, and Co were respectively $(1.4331\pm0.0036)\times10^5$, $(1.5494\pm0.0034)\times10^5$, and $(1.5743\pm0.0040)\times10^5$ J/mol, while those for the backward reactions were $(5.3307\pm0.0041)\times10^5$, $(2.4753\pm0.0093)\times10^5$, and $(1.6289\pm0.0092)\times10^5$ J/mol, respectively. The leaching mechanism was found to be exothermic, which allows maximum recovery at low temperatures. The findings highlight ammonia's effectiveness as a selective leachant, significantly reducing manganese in the leaching solution, and streamlining nickel and cobalt separation, thus enhancing the recycling process's efficiency and sustainability.*

Keywords: *NMC battery; recycling; ammonia leaching; kinetics; thermodynamics*

■ INTRODUCTION

In recent years, lithium-ion batteries (LIBs) have been widely used as a portable power source in various electronics, in electric vehicles (EVs) and as a stationary storage for renewable energies [1-2]. Even though the battery is rechargeable, the lifetime of a LIB is typically limited to about 1–3 years for electronic devices [3-4] and 5–8 years for EVs or energy storage systems [3,5]. LIBs that have reached their usage limits will become waste and may pose a danger to humans and the environment [6-7]. The massive use and increasing demand for LIBs will surely result in a large quantity of battery waste in the future.

It is predicted that by 2040, the quantity of spent LIBs will reach more than 8 million tons [7-8], a situation that requires a comprehensive solution. Battery recycling is considered an appropriate approach because it fosters a circular economy of LIB components and reduces the need to source battery precursors from nature [9]. However, battery recycling is challenging because of the complexity of the physical and chemical properties of the components in a spent battery. For this reason, the rate of LIB recycling achieved in the European Union is only about 5% [10]. This low progress is mostly due to the relatively large cost of the recycling process. Therefore, developing more efficient, economically feasible, and environmentally friendly battery recycling technology is necessary.

Currently, the most common LIB recycling processes involve pyrometallurgy and hydrometallurgy or a combination of both [11]. In pyrometallurgy, metal recovery is carried out at high temperatures (> 1000 °C). This process is considered environmentally unfriendly

because it requires a lot of energy and produces massive carbon emissions. For the extraction of metals from spent LIB, hydrometallurgy is considered the most appropriate method. In the hydrometallurgy process, metals are extracted using chemicals or microorganisms in a two-stage process of selective leaching and selective precipitation [12]. Recycling spent LIBs through hydrometallurgy is preferrable because the process is relatively simple and has a more controllable environmental impact than pyrometallurgical processes.

Leaching is an important stage in metal recovery from spent LIBs. The metals can dissolve in a solution of chemical reagents such as sulfuric acid [13-14], hydrochloric acid [15-16], nitric acid [17], phosphoric acid [18], ammonia [19-22], maleic acid [23], ascorbic acid [24-25], and citric acid [26]. In the case of bioleaching, microorganisms such as *Acidithiobacillus ferroxidans* [27] and mesophilic potential sulfur-oxidizing bacteria [28] are used to help extract the metals. However, chemical leaching is still considered a simpler and faster process compared to bioleaching [29]. Extracting metals with chemical reagents has become the most preferred process in the LIB recycling. However, the separation of dissolved metals remains challenging in achieving high recovery and purity of the final product. Although the leaching process might dissolve all metals, it would require a lengthy and complex separation process. Due to its high complexity, even separation using a nanofiltration membrane is still difficult to produce a complete metal separation [30], which becomes challenging to employ in industrial applications. Therefore, a selective leaching would help ease the burden of separation.

The chemical reagent used in the selective leaching process depends on the type of LIB cathode material. There are several types of commercialized LIBs, including lithium manganese cobalt oxides (NMC), lithium nickel cobalt aluminium oxides (NCA), lithium manganese oxides (LMO), lithium cobalt oxides (LCO), and lithium iron phosphate (LFP) [31] among which NMC is the one widely used for EVs due to its large energy density [32]. However, because nickel and cobalt are expensive, NMC is often combined with LMO to reduce production costs while maintaining the energy density [33-34]. Currently, several EVs have already adopted the NMC-LMO type battery, such as the Nissan Leaf (BEV), Chevrolet Volt (PHEV), and BMW i3 (BEV) [34]. The combined NMC-LMO battery is often called a lithium manganese-rich (LMR) battery.

In the NMC-LMR cathodes, the manganese content is around 3× higher than that of lithium. The fact that manganese can be present as multivalent in the solution might lead to complications in separating manganese from other metals, especially when the separation occurs through multistage precipitation. A large amount of manganese requires a lot of precipitation reagent, which makes the process uneconomic and highly likely to contaminate the lithium products. Therefore, a selective leaching technique for NMC-LMR-type cathodes needs to be developed. Besides reducing the need for the reagent and avoiding impurities, selective leaching can reduce the burden on the separation process.

Organic acids such as citric acid [35], ascorbic acid [36], acetic acid [37], and oxalic acid [38] are commonly used for selective leaching. Since organic acids provide a moderate pH level and have the ability to form metal complexes, they might selectively dissolve metals. However, compared to inorganic acids, organic acids are more expensive, making the leaching process less economical. Therefore, an alternative inexpensive reagent, such as weak base ammonia (NH_3), can be used to selectively extract the metals from LIB cathodes. Leaching studies with NH_3 have been reported to selectively leach metals from LIB cathodes. A mixture of NH_3, $(NH_4)_2CO_2$, and $(NH_2)_2SO_2$ as a leaching agent was studied in a selective ammonium leaching for NMC-422 type batteries [20]. Thermal treatment of spent NMC-111 cathode at 550 °C before leaching was also studied to help metal extraction using a mixture of NH_3, $(NH_4)_2CO_3$, and $(NH_4)_2SO_3$ [21], as well as in a mixture of NH_3, Na_2SO_3, and $(NH_4)_2SO_4$ [19]. In addition, ammonium leaching was used to leach cathode materials of NMC-111, NMC-532, and NMC-811 using a mixed reagent of NH_3, Na_2SO_3, and NH_4Cl [22]. The experimental results showed that the manganese was insoluble and remained in the residue. However,

ammonium leaching performance has never been evaluated for LMR-NMC type LIB cathodes containing much higher manganese composition.

The present work studied the characteristics of ammonium leaching for the cathodes of spent LMR-NMC type LIB batteries. The performance of ammonia leaching on Li, Ni, Mn, and Co recovery was studied using a mixture of reagents containing NH_4OH, Na_2SO_3, and $(NH_4)_2SO_4$ at various concentrations and temperatures. It was expected that the leaching agents could leach Li, Ni, and Co while effectively preventing Mn from being present in the leaching solution. The experimental data were then used to explain the leaching mechanism. In addition, the data were also used to evaluate kinetic parameters of the proposed mathematical model. Thermodynamic parameters of the leaching process were also evaluated.

■ EXPERIMENTAL SECTION

Materials

Spent LIBs from the electric motor vehicle PT VIAR Indonesia, a local automotive manufacturer, were used as raw materials. In this study, the reagents used included sodium chloride (NaCl, technical grade, Refina), 96–97% sulfuric acid (H_2SO_4, EMSURE for analysis, Merck Millipore), 30% hydrogen peroxide (H_2O_2, EMSURE for analysis, Merck Millipore), 25% ammonium solution (NH_4OH, EMSURE for analysis, Merck Millipore), sodium sulfite anhydrous (Na_2SO_3, EMSURE for analysis, Merck Millipore), and ammonium sulphate anhydrous ($(NH_4)_2SO_4$, EMSURE for analysis, Merck Millipore). In addition, demineralized water was used for battery discharging, cathode leaching, dissolving reagents, and diluting samples for sample preparation before the characterization.

Instrumentation

The concentration of elements in the solution was analyzed using inductively coupled plasma optical emission spectrometry (ICP-OES Optima 8300, Perkin Elmer). In case of solid samples, the samples were first dissolved using a microwave digester (Titan MS, Perkin Elmer) and diluted before being analyzed with ICP-OES. Raman microscope spectrometer (UV–vis–NIR Dispersive Micro Confocal Hyperspectral Raman Imaging Spectrometer, Horiba) was used to analyze the presence of compounds in the solid samples with setting parameters of 100× magnification objective lens, 532 nm laser, 100.021 holes, 600 grating, 25% ND filter, and an acquisition time of 40 s.

Procedure

Cathode material preparation

Some steps of pretreatment were conducted to obtain cathode materials used in this work. The pretreatment steps are illustrated in Fig. 1. Spent battery cells were first discharged by immersion in a 1 M NaCl salt solution for 48 h. After discharging, battery cells were dismantled to obtain cathode sheets. The cathode sheet is comprised of aluminium and coated with an active cathode material. The active cathode material was separated from the aluminium sheet by immersing it in a low-concentration acid solution to dissolve the binder. A total of 10.8831 g of battery cathode sheets were taken and immersed in 200 mL of 0.2 M H_2SO_4 to separate the cathode material from the aluminium. The process was assisted by 1000 rpm stirring with a stirrer motor (RW-20, IKA) equipped with four turbine blades. Stirring was conducted for 20 min at room temperature. The aluminium sheet was then separated from the cathode slurry with a 25 mesh screener. The cathode slurry was filtered with a 2.5 µm filter paper (Whatman 42) in a Buchner funnel equipped with a vacuum pump (RV5, Edwards). The filtered cathode was then dried in an oven (UN55, Memmert) at 110 °C for 2 h.

Ammonia leaching

All leaching experiments used a total liquid volume of 250 mL with 2.5 g of solid powder. The leaching process was carried out in a 500 mL three-necked round-bottomed flask (Pyrex) equipped with a reflux condenser to avoid liquid loss due to evaporation. The leaching container was equipped with a 4-turbine blade stirrer (RW-20, IKA), temperature indicator and a mantle heater (MS-E 103, MTOPS) with a temperature control. The leaching process is illustrated in Fig. 1. A 25% NH_4OH solution was mixed with Na_2SO_3, and $(NH_4)_2SO_4$

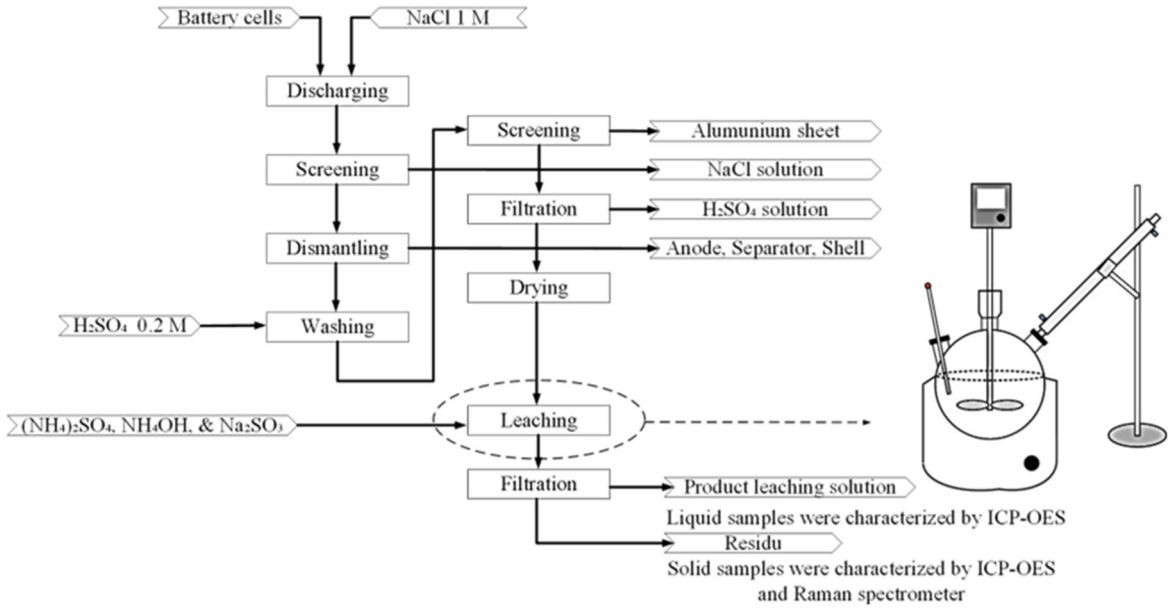

Fig 1. Flow diagram of the experimental method

to form 250 mL of a mixture containing 1 M NH_4OH, 1 M Na_2SO_3, and various concentration of $(NH_4)_2SO_4$ solution. The concentration of $(NH_4)_2SO_4$ in the solution was varied to 1.0, 1.5, and 2.0 M. The leaching solution was prepared in a 250 mL volumetric flask with shaking until the mixture completely dissolved to form a homogeneous solution. The leaching solution was put into a 500 mL three-necked round-bottomed flask and heated to operating temperature conditions using a heating mantle. The operating temperature was varied to 50, 60, 70, and 80 °C. After the operating condition was reached, 2.5 g of cathode powder was put into the leaching solution in the flask. The solution was sampled sequentially after 10, 30, 60, 120, and 180 min and then filtered through a 0.2 µm syringe filter to analyze the concentration of four specific metals (Li, Ni, Mn, and Co) in the cathode material.

Material characterization

Liquid and solid samples were taken from the leaching process. Liquid samples taken each time were analyzed to determine the concentration of elements Li, Ni, Mn, and Co in the solution using ICP-OES. Each 200 µL liquid sample was diluted with demineralized water up to 10 mL for the analysis. The sample was stirred using a vortex mixer (MX-S, DLAB) until a homogeneous solution was observed. Meanwhile, solid samples were also characterized to determine the concentrations of Li, Ni, Mn, and Co. The solid samples, including cathode powder and leaching residue, were first dissolved using a microwave digester and then diluted before being analyzed with ICP-OES. The compounds present in the solid samples were then analyzed using Raman microscope spectrometer.

Leaching kinetics and thermodynamics analysis

This present work also aimed to evaluate appropriate leaching mechanism and kinetic model based on experimental data. Recovery of metals from the cathode material through ammonia leaching generally includes reduction, dissolution, complexation and precipitation. The reduction process is triggered by a reducing agent of Na_2SO_3. The activation mechanism of Na_2SO_3 as a reducing agent is shown in Eq. (1–3) [39]. Oxidation of SO_3^{2-} causes the release electrons, which are then received by the high-valence metals.

$$Na_2SO_{3_{(s)}} \rightleftharpoons 2Na^+_{(aq)} + SO^{2-}_{3\ (aq)} \quad (1)$$

$$SO^{2-}_{3\ (aq)} \rightleftharpoons SO_{3_{(aq)}} + 2e^- \quad (2)$$

$$SO_{3_{(aq)}} + 2NH_4OH_{(aq)} \rightleftharpoons (NH_4)_2\,SO_{4_{(aq)}} + H_2O_{(aq)} \quad (3)$$

The reduction process in the LMR-NMC cathode system occurs by lowering the oxidation number of the high-valence transition metals to the lowest state, as shown in Eq. (4–9).

$$aLiMn_2O_4 \cdot bLiNi_xMn_yCo_{1-x-y}O_{2_{(s)}} \rightarrow aLiMn_2O_{4_{(s)}} + bLiNi_xMn_yCo_{1-x-y}O_{2_{(s)}} \quad (4)$$

$$LiMn_2O_{4_{(s)}} \rightarrow Li^+_{(s)} + Mn^{3+}_{(s)} + Mn^{4+}_{(s)} + 4O^{2-} \quad (5)$$

$$LiNi_xMn_yCo_{1-x-y}O_{2_{(s)}} \rightarrow Li^+_{(s)} + xNi^{m+}_{(s)} + yMn^{n+}_{(s)} + (1-x-y)Co^{o+}_{(s)} + 2O^{2-} \quad (6)$$

$$Ni^{m+}_{(s)} + (m-2)e^- \rightarrow Ni^{2+}_{(s)} \quad (7)$$

$$Co^{o+}_{(s)} + (o-2)e^- \rightarrow Co^{2+}_{(s)} \quad (8)$$

$$Mn^{n+}_{(s)} + (n-2)e^- \rightarrow Mn^{2+}_{(s)} \quad (9)$$

The reduction would bring the metals Ni, Co, and Mn to the lowest oxidation stage, which is 2+, while Li remains at 1+. Ni and Co with a lower valence easily dissolve and form complexes upon reaction with NH_3 [19-21]. Eventually, the leaching process produces Li in a stable ionic, while Ni and Co remain stable as metal complexes in the liquid phase. Mn is known to have very poor complexation properties with amines [20], leading it to react with hydroxides at alkaline pH. This interaction forms manganese hydroxide, which immediately precipitates and stabilized in a solid phase. The mechanism of the metals' dissolution, complexation, and precipitation of manganese follows Eq. (10–15).

$$2Li^+_{(s)} + (NH_4)_2SO_{4_{(aq)}} \rightleftharpoons Li_2SO_{4_{(aq)}} + 2NH^+_{4_{(aq)}} \quad (10)$$

$$2Ni^{2+}_{(s)} + 6(NH_4)_2SO_{4_{(aq)}} \rightleftharpoons 2Ni(NH_3)^{2+}_{6_{(aq)}} + 6H_2SO_{4_{(aq)}} \quad (11)$$

$$2Co^{2+}_{(s)} + (NH_4)_2SO_{4_{(aq)}} \rightleftharpoons 2Co(NH_3)^{2+}_{(aq)} + H_2SO_{4_{(aq)}} \quad (12)$$

$$Mn^{2+}_{(s)} + (NH_4)_2SO_{4_{(aq)}} \rightleftharpoons MnSO_{4_{(aq)}} + 2NH^+_{4\,(aq)} \quad (13)$$

$$MnSO_{4_{(aq)}} + 2NH_4OH_{(aq)} \rightleftharpoons Mn(OH)_{2_{(s)}} + (NH_4)_2SO_{4_{(aq)}} \quad (14)$$

$$H_2SO_{4_{(aq)}} + 2NH_4OH_{(aq)} \rightleftharpoons (NH_4)_2SO_{4_{(aq)}} + 2H_2O_{(aq)} \quad (15)$$

The leaching mechanism was evaluated by a kinetic model. The cathode leaching process involves several reaction steps: reduction initiation, metal reduction, metal dissolution, ion complexation, and precipitation. In this reaction process, the metal reduction step is generally spontaneous and does not control the process. The complexation process is also considerably fast because it stabilizes only Ni and Co metals within the liquid system. The complexation will also not change the observable concentrations of metal elements Ni and Co in the liquid, making them difficult to evaluate. Therefore, the leaching kinetics were mainly based on the controlling reactive dissolution step. The dissolution model could be approached with the equilibrium-shrinking core model [40] by applying the following assumptions. (i) The liquid was well agitated to maintain a homogeneous concentration in the liquid body. (ii) Turbulence in the liquid body causes a negligible resistance of the liquid film on the solid surface. (iii) Particles were spherical and uniformly distributed, in which a pseudo-homogeneous reaction is controlling. (iv) Ammonia leaching agent was relatively abundant so the concentration is constant.

Mathematical model of the kinetics

The reactive dissolution model is approached by an equilibrium reaction model as in Eq. (16).

$$A^{p+}_{(s)} + bR_{(aq)} \rightleftharpoons AR^{p+}_{b\ (aq)} \quad (16)$$

The overall reaction in equations can be written as Eq. (17).

$$\left(-R_{A^{p+}_{(s)}}\right) = k_1 C_{A^{p+}{}_{(s)}} C_{R_{(aq)}} - k_2 C_{AR^{p+}_{b\ (aq)}} \quad (17)$$

Eq. (17) can be expressed in term of the metal recovery as expressed in Eq. (18–21).

$$\left(-R_{A^{n+}_{(s)}}\right) = -\frac{dN_{A^{n+}_{(s)}}}{dt} = k_1 C_{A^{p+}{}_{(s)}} C_{R_{(aq)}} - k_2 C_{AR^{p+}_{b\ (aq)}} \quad (18)$$

$$-\frac{d\left(N^0_{A^{n+}_{(s)}}(1-X_A)\right)}{dt} = k_1 \frac{N^0_{A^{p+}{}_{(s)}}}{V_p}(1-X_A) - \frac{k_2 N^0_{A^{p+}_{(s)}}}{V_R} X_A \quad (19)$$

$$\frac{d(X_A)}{dt} = \frac{k_1 C_{R_{(aq)}}}{V_p}(1-X_A) - \frac{k_2}{V_R} X_A \quad (20)$$

$$\frac{d(X_A)}{dt} = k_f(1-X_A) - k_b X_A \quad (21)$$

The profile of metal A recovery (X_A) can be obtained by solving numerically Eq. (21) with an initial condition (t = 0) where metal A is still absent in the solution $(X_{A_0} = 0)$.

Kinetics parameter analysis

The forward and backward reaction rate constants are temperature dependent, and their correlation follows the modified Arrhenius equation [41]. This modification can be derived from the van't Hoff equation [42] to get the final form of Eq. (22).

$$k = AT^{m} \exp\left(-\frac{E_a}{RT}\right) \tag{22}$$

The constant (m) is empirical to approach experimental data. The constant parameters in Eq. (21) and (22) were evaluated by fitting experimental data in various operating conditions. The final Eq. (23) was used for the parameter fitting process.

$$\frac{d\left(X_A\big|_{T_{(i)}}\right)}{dt} = A_f T_{(i)}^{m_f} \exp\left(-\frac{E_{a_f}}{RT_{(i)}}\right)\left(1-X_A\right) - A_b T_{(i)}^{m_b} \exp\left(-\frac{E_{a_b}}{RT_{(i)}}\right)X_A \tag{23}$$

The A_f, A_b, m_f, m_b, E_{a_f}, and E_{a_b} parameters are assumed constant. They are evaluated by minimizing the difference between simulated metal recovery and experimental data through the sum of squares of errors (SSE) and Jacobian matrices, using the lsqnonlin function in MATLAB toolboxes.

Thermodynamics parameter analysis

In this work, we observed that the leaching process did not achieve complete recovery. The leaching process reaches equilibrium when the change of recovery over time $\left(\frac{d(X_A)}{dt} = 0\right)$. The equilibrium constant can be defined as follows in Eq. (24) and (25).

$$\frac{d\left(X_A\right)}{dt} = k_f\left(1-X_{A_E}\right) - k_b X_{A_E} = 0 \tag{24}$$

$$K(T) = \frac{k_f(T)}{k_b(T)} = \frac{X_{A_E}}{\left(1-X_{A_E}\right)} \tag{25}$$

At equilibrium, the Gibbs free energy of the system reaches a minimum so that the change in the Gibbs free energy of the system (ΔG) becomes zero, as shown in Eq. (26) and (27).

$$\Delta G = \Delta G^0 + RT \ln K \tag{26}$$

$$\Delta G^0 = -RT \ln K \tag{27}$$

The change in Gibbs free energy at standard condition (ΔG^0) can be correlated with other thermodynamic parameters such as enthalpy (ΔH^0) and entropy (ΔS^0), as shown in Eq. (28). The correlation can be linearized across various temperature variations.

$$-\frac{\Delta H^0}{R}\left(\frac{1}{T}\right) + \frac{\Delta S^0}{R} = \ln K \tag{28}$$

■ RESULTS AND DISCUSSION

Raw Material Characterization

Table 1 shows the composition of cathode materials used in this study. The cathode material contains 48.03% manganese, 27.87% nickel, 11.48% cobalt, 7.52% lithium, 4.36% aluminium, and 0.74% iron. Aluminium and iron are not actually from the cathode's active materials. Aluminium is the sheet material coated with the cathode active materials. The cathode sheet material may be carried out due to imperfect pretreatment processes. Meanwhile, the iron content might come from the battery's steel shell, small fraction of which remains in the resulting powder during the pretreatment stage. As seen in Table 1, manganese constitutes the largest portion of cathode material at 48.03%. Therefore, the battery cathode in this study can be categorized as a modified NMC with the addition of LMO cathode material. This cathode type is often called LMR-NMC, which in this work combines 1/3 LMO ($LiMn_2O_4$) and 2/3 NMC-532 ($LiNi_{0.5}Mn_{0.3}Co_{0.2}O_2$). The presence of LMO material in the cathode material is also indicated by a Raman shift at 654.50 cm^{-1}, as shown in Fig. 2, which corresponds to $LiMn_2O_2$ spinel [43].

Table 1. The metal composition of the cathode material

Elements	Concentration (% w/w)
Nickel	27.87
Lithium	7.52
Cobalt	11.48
Iron	0.74
Aluminium	4.36
Manganese	48.03

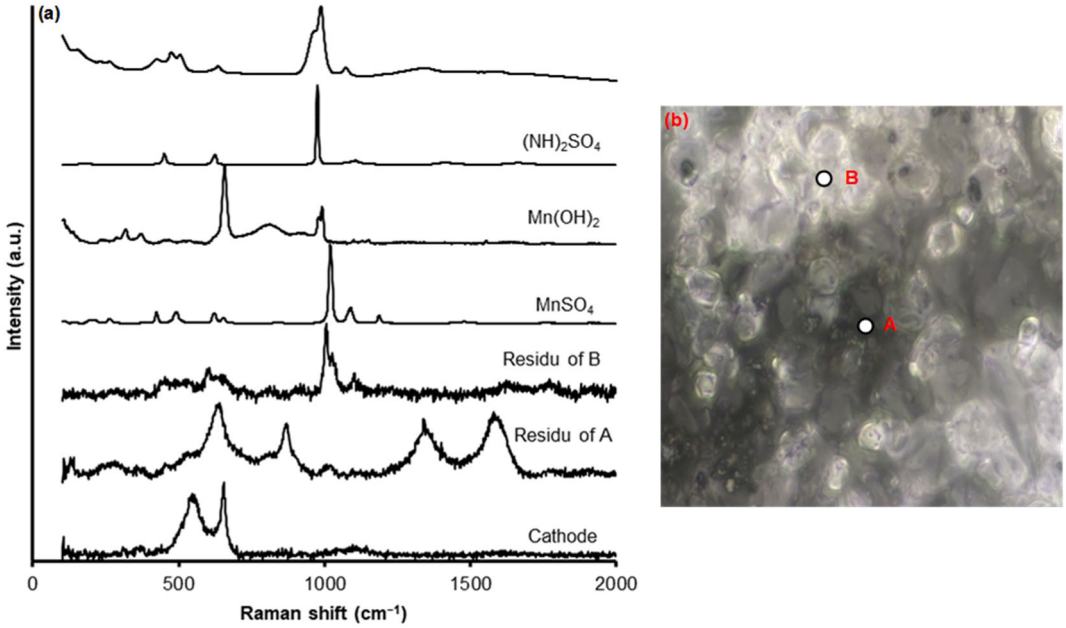

Fig 2. Raman spectroscopy analysis (a) Raman spectra of leaching residues and standard compounds, (b) position (A) and (B) at which spectra were taken from the samples

Leaching Mechanism

The ammonia leaching process for dissolving cathode metals is a highly complex process that involves numerous substances. The reaction mechanism of ammonia leaching of LMR-NMC cathode comprises a series of reactions, including initiation of the reducing agent, reduction, dissolution, complexation, and precipitation of metals.

In this study, the dissolved Na_2SO_3 produces ions that act as a reducing agent, as depicted in Eq. (1-3). First, Na_2SO_3 ionizes in water to form SO_3^{2-} [39], which acts as a reducing agent that can reduce transition metals such as Ni, Mn, and Co through redox reactions outlined in Eq. (7-9). The solubility of Na_2SO_3 increases with temperatures, leading to a faster and easier start of the metal reduction process. After the formation of reducing ions, metals in the LMR-NMC cathode can be reduced to a lower valence state, making them more readily dissolved in an ionic solvent. Lithium is stable in an ionic form, while nickel and cobalt transition metals interact with ammonia to form complex ions [19-21]. Nickel forms a complex with six ammonia molecules, while cobalt forms a complex with one ammonia molecule. The complex compounds of nickel and cobalt with ammonia are stable in the aqueous phase, as indicated by the Pourbaix diagram in Fig. 3(a) and (b).

In ammonia leaching, manganese undergoes a different mechanism than the transition metals of nickel and cobalt. Manganese leached in the ionic form is not easily complexed with ammonia, but it reacts with the hydroxide ions in the solution to form manganese hydroxide ($Mn(OH)_2$). In addition, a high concentration of ammonia and sulfite ions can trigger Mn ions to precipitate in the form $(NH_4)_2Mn(SO_3)_2$. The $(Mn(OH)_2)$ and $(NH_4)_2Mn(SO_3)_2$ precipitates were observed in the Raman spectra of the residue that remained after the leaching, as shown in Fig. 2.

The presence of $Mn(OH)_2$ in the residues was identified from Raman shifts at 532 (A), 640 (A), 813 (B), and 917 cm^{-1} (B). The Raman shift at 640 cm^{-1} indicates a symmetric vibration Mn–O [44]. Meanwhile, the compound $(NH_4)_2Mn(SO_3)_2$ was identified at Raman shifts of 384 (A), 451 (A and B), 1414 (B), 1663 (B), 1005 (B), and 1102 cm^{-1} (B). The Raman shift at 384 and 451 cm^{-1} indicate the vibration modes of ammonia [45]. The Mn compound residue detected in the form of double sulfite from ammonia leaching was also identified in another study using XRD analysis, which

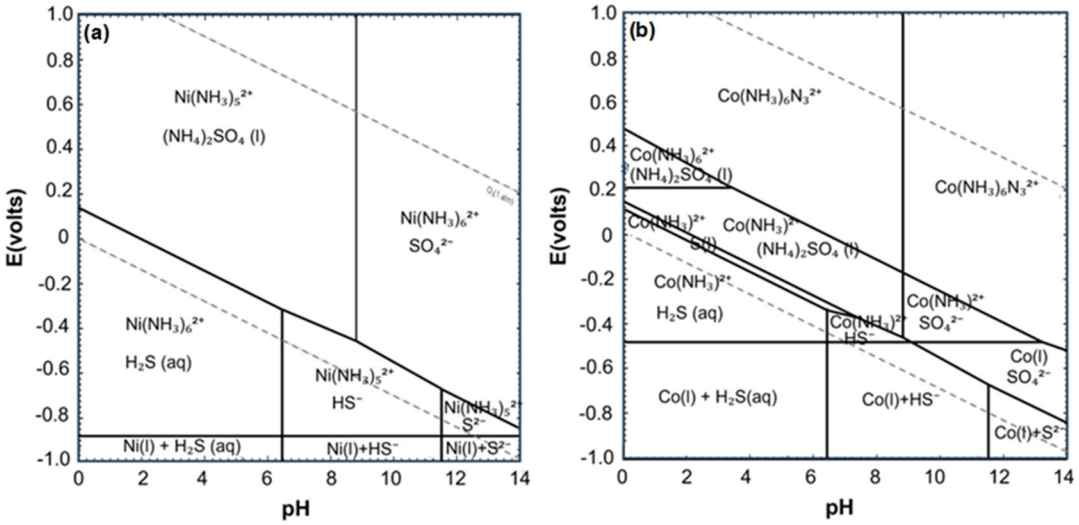

Fig 3. Pourbaix diagram (a) Ni-N-S-H_2O systems and (b) Co-N-S-H_2O systems

suggested the presence of hydrates in the form of $(NH_4)_2Mn(SO_3)_2{\cdot}H_2O$ [19]. The Raman shifts at 1340 (A) and 1580 cm^{-1} (A) in this study suggested the presence of carbon in the cathode material. Based on the aforementioned results, the mechanism of Mn compound precipitates formation in the residue in the ammonia leaching can be described by Eq. (32) and (33).

$$Mn^{2+}_{(aq)} + 2NH_4OH_{(aq)} \rightleftharpoons Mn(OH)_{2_{(s)}} + 2NH^{+}_{4\,(aq)} \quad (32)$$

$$Mn^{2+}_{(aq)} + 2NH^{+}_{4\,(aq)} + 2Na_2SO_{3_{(aq)}} \rightleftharpoons (NH_4)_2\,Mn(SO_3)_{2_{(s)}} + 4Na^{+}_{(aq)} \quad (33)$$

Effect of $(NH_4)_2SO_4$ Concentration

In this study, three concentrations of $(NH_4)_2SO_4$ were used to experimentally investigate the effect of the concentration on the recovery of Li, Ni, Mn, and Co from the spent LMR-NMC cathode material. The experiments were carried out at a constant solid/liquid ratio of 10 g/L, 1 M NH_3, 1 M Na_2SO_3 as reducing agent, and at leaching temperature of 70 °C. As shown in Fig. 4, the $(NH_4)_2SO_4$ concentration positively affects the recovery of Li, Ni, and Co in the ammonia leaching. Although the increase was not significant, the concentration of $(NH_4)_2SO_4$ could

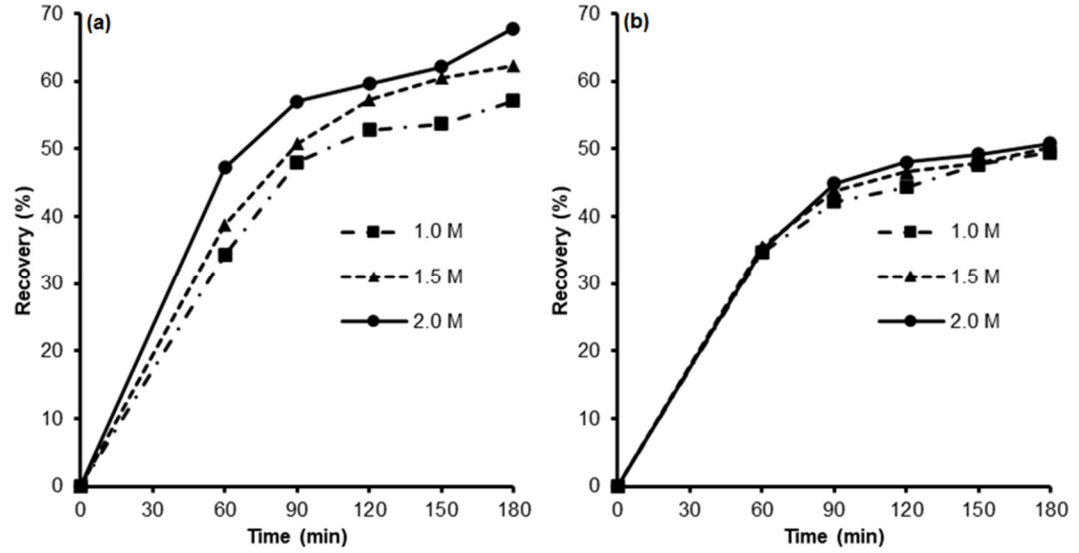

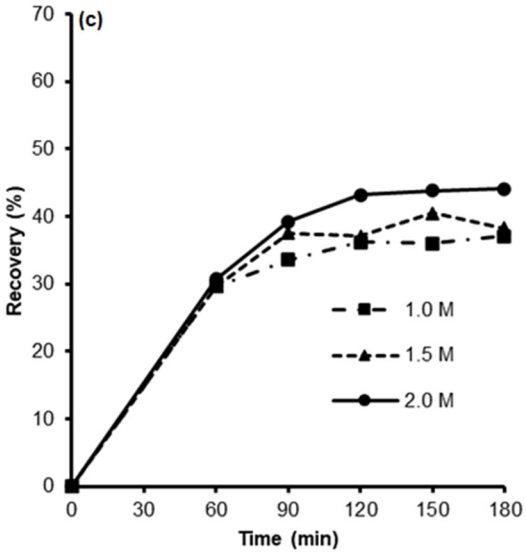

Fig 4. Leaching recovery at various $(NH_4)_2SO_4$ concentrations for (a) Li, (b) Ni, and (c) Co

increase the recovery of Li, Ni, and Co up to 10%. At a concentration of 1 M, the leaching process exhibits a recovery of Li, Ni, and Co of 57.12%, 49.45%, and 37.09%, respectively. The recovery of Li, Ni, and Co experiences a further increase to 62.30, 50.24, and 38.26, respectively, at a concentration of 1.5 M. Meanwhile, as the concentration was raised to 2 M, the leaching performance continued to increase to reach a recovery of Li, Ni, and Co up to 67.76, 50.84, and 44.05%, respectively.

As shown in Fig. 4, the recovery of Mn in the solution was not observable at various concentrations of $(NH_4)_2SO_4$. The Mn was found to be stable as a compound remained in the solid phase. Due to its poor complexation with ammonia, Mn might precipitate mostly in the form of hydroxides. As shown in Fig. 2, Raman spectra show that the manganese compounds in the residue are found in the form of $Mn(OH)_2$ and $(NH_4)_2Mn(SO_4)_2$. This result suggests that Mn in the ammonium leaching will first be extracted from the cathode material into the solution. However, since the system is in alkaline condition, rich in hydroxide ions, the Mn ions are most likely to react with hydroxide to form precipitated $Mn(OH)_2$. In addition, because the solution also contains a high concentration of ammonium and sulphate ions, Mn also form $(NH_4)_2Mn(SO_4)_2$ precipitates. This phenomenon is obvious during transient observation, as shown in Fig. 5. Mn shortly appears in the solution but then precipitates, becoming $Mn(OH)_2$ and $(NH_4)_2Mn(SO_4)_2$. The precipitation rate appears to be relatively faster than the leaching rate, so the concentration of Mn in the solution is observable only for a very short duration. The concentration increases in the beginning but then decreases to a negligible level due to fast precipitation. It is known that the solubility of $Mn(OH)_2$ is very low, at 0.0028 g/L or has a K_{sp} value of 1.3×10^{-13} [46]. In contrast, Ni and Co do not form precipitates because their ions are complexed with ammonium, forming cobalt ammonium and nickel ammonium complexes that remain stable in the solution.

The increase of $(NH_4)_2SO_4$ concentration in the leaching solution will lower the pH and increase the reduction potential (Eh) of the solution. In this study, the pH resulting from the addition of $(NH_4)_2SO_4$ at concentrations of 1.0, 1.5, and 2.0 M ranges from 10.5, 9.0 to 8.5. At lower pH and higher Eh, the solution becomes more reactive and able to facilitate the dissolution of high-valence metals such as Ni, Co, and Mn. Therefore, this study finds that an increase in $(NH_4)_2SO_4$ leads to increased metal recovery. At higher Eh level, the solution becomes reductive, and able to reduce high-valence metals such as Ni, Co, and Mn, thereby weakening the bonds of metals within the cathode material. Once the high-valence metals are dissolved, Li also dissolves more readily. The ease with which high-valence metals to

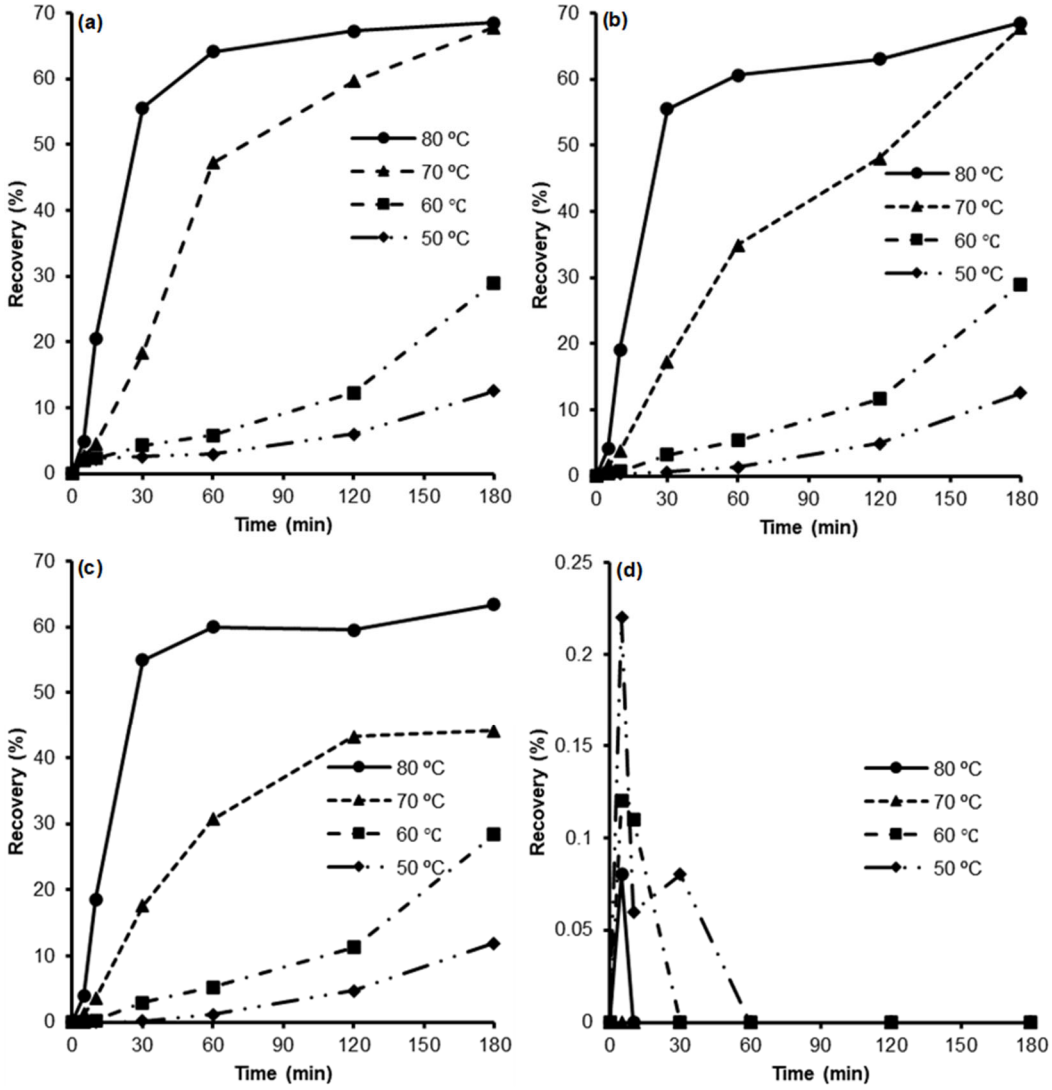

Fig 5. Leaching recovery at various temperatures for (a) Li, (b) Ni, (c) Co, and (d) Mn

dissolve in the ammonia solution agrees with the Eh-pH thermodynamic diagram study of Co-N-S-H_2O and Ni-N-S-H_2O systems at a temperature of 70 °C, as shown in Fig. 3.

The highest metal leaching recovery was achieved using $(NH_4)_2SO_4$ with a concentration of 2 M (pH level of 8.5). The addition of $(NH_4)_2SO_4$ with a concentration of 2 M produced a stable compound in the form of a cobalt complex $Co(NH_3)^{2+}$ in the solution, as indicated by the Eh-pH simulation of the Co-N-S-H_2O system. Similarly, based on the Eh-pH diagram of the Ni-N-S-H_2O system, the stable phase of Ni in the ammonium leaching system is the complex ion $Ni(NH_3)_6^{2+}$. The thermodynamics illustrated in the Eh-pH diagram in Fig. 3(a-b) indicate that the dissolution of Ni and Co metals occurs spontaneously and stably in ionic complexes in the solution. In contrast, Mn is difficult to complex with ammonia and instead precipitates to form a stable $Mn(OH)_2$ and $(NH_4)_2Mn(SO_4)_2$.

Effect of Temperature Operations

To investigate the effect of temperature on the recovery of Li, Ni, Mn, and Co metals in the LMR-NMC cathode leaching process, experiments were conducted at four different temperatures. The experiments were carried out at a constant solid/liquid ratio of 10 g/L, 1 M NH_3, 1 M Na_2SO_3, and 2 M $(NH_4)_2SO_4$. The temperatures used were 50, 60, 70, and 80 °C. The results of metal

recovery are shown in Fig. 5. As depicted in Fig. 5, an increase in temperature resulted in a higher recovery for Li, Ni, and Co in a 180-min leaching period. An increased temperature led to faster chemical reactions, as indicated by the increased recovery per unit of time. The faster reaction leads to a quicker achievement of equilibrium conditions at high temperatures, as observed in the recovery trend at 80 °C. However, Fig. 5 indicates that the recovery of Ni and Co at lower temperatures is expected to continue increasing beyond the leaching duration period.

At a temperature of 50 °C, in the same leaching period of 180 min, the leaching process yielded recovery rates of 12.52% for Li, 11.87% for Ni, and 11.96% for Co. At 60 °C, the metal recovery of Li, Ni, and Co increased to 28.96%, 28.76%, and 28.38%, respectively. As the temperature was raised to 70 °C, the metal recovery of Li, Ni, and Co increased significantly to 67.76%, 50.84%, and 44.05%, respectively. The sharp increase in leaching recovery is likely due to a temperature shift from 60 to 70 °C. A further temperature rise to 80 °C causes a continuous metal recovery increase of Li, Ni, and Co to 68.46%, 65.57%, and 63.34%, respectively, but seems to reach equilibrium more quickly.

Fig. 5 shows that the higher the temperature, the faster the reaction. An increase in temperature can trigger an increase in the kinetic energy of the molecules so that the frequency of collisions between molecules increases [47]. The Maxwell-Boltzmann equation can explain the increase of kinetic energy due to temperature rise [48-49]. In this study, the frequency of collisions increases and accelerates the reaction to form more leaching products. Besides, temperature increases seem to positively influence the metal reduction steps. This was indicated by a sharp increase in recovery and rate of reaction between 60 and 70 °C. The dissociation of Na_2SO_3 into SO_3^{2-}, which acts as a reducing agent for metals in the leaching process is likely to occur more actively at temperatures above 60 °C. This suggests that activation energy for metals reduction needs to be overcome to allow redox reaction using Na_2SO_3 to occur. This would explain a shift in the regime of reaction mechanism between 60 and 70 °C. Below 60 °C, the reaction might proceed without the role of Na_2SO_3, which results in a low rate of metal recovery. Meanwhile, above 60 °C, the metal reduction would take place with the involvement of Na_2SO_3, which provide SO_3^{2-}, leading to a faster reaction rate of metal recovery. However, in the case of Mn, as shown in Fig. 5, the effect of temperature on the leaching rate seems to be overshadowed by the rate of its precipitation. The precipitation of Mn from the solution occurs much faster than its leaching step with increasing temperature. As shown in Fig. 5, the recovery of Mn was observed to peak, and the presence in the solution disappeared after a while. It was observable that the concentration of Mn in the solution was higher at low temperatures, and its presence lasted longer than at higher temperatures.

Leaching Kinetics

Leaching kinetic parameters of the LMR cathode using ammonia were evaluated by solving the kinetics model in Eq. (25). The kinetic parameters, including activation energy (E_a), frequency factor (A) and the order of temperature in the modified Arrhenius equation (m), were determined. The parameter fitting was conducted by minimizing the SSE between experimental data and simulated recovery, using the lsqnonlin toolbox in MATLAB. Fig. 6 shows a good agreement between the calculated recovery and the experimental data. The determination coefficient (R^2), whose value is close to unity (0.9504 for Li, 0.9640 for Ni and 0.9616 for Co), indicates that the proposed kinetic model appropriately represents the leaching kinetics.

As depicted in Fig. 6, the proposed model can perfectly simulate the progress of Li, Ni, and Co recoveries with time, which is close to the experimental data. The leaching mechanism consists of parallel reactions of individual metal. However, the increase of reaction rate with temperature between 60 and 70 °C occurs much more rapidly, so the conventional Arrhenius correlation is insufficient to approach experimental data. A modified Arrhenius derived from the van't Hoff equation is used in the model as expressed in Eq. (24). The temperature-dependent modified Arrhenius correlation can fit the experimental data with relatively small SSE and R^2. The reliability of the proposed model

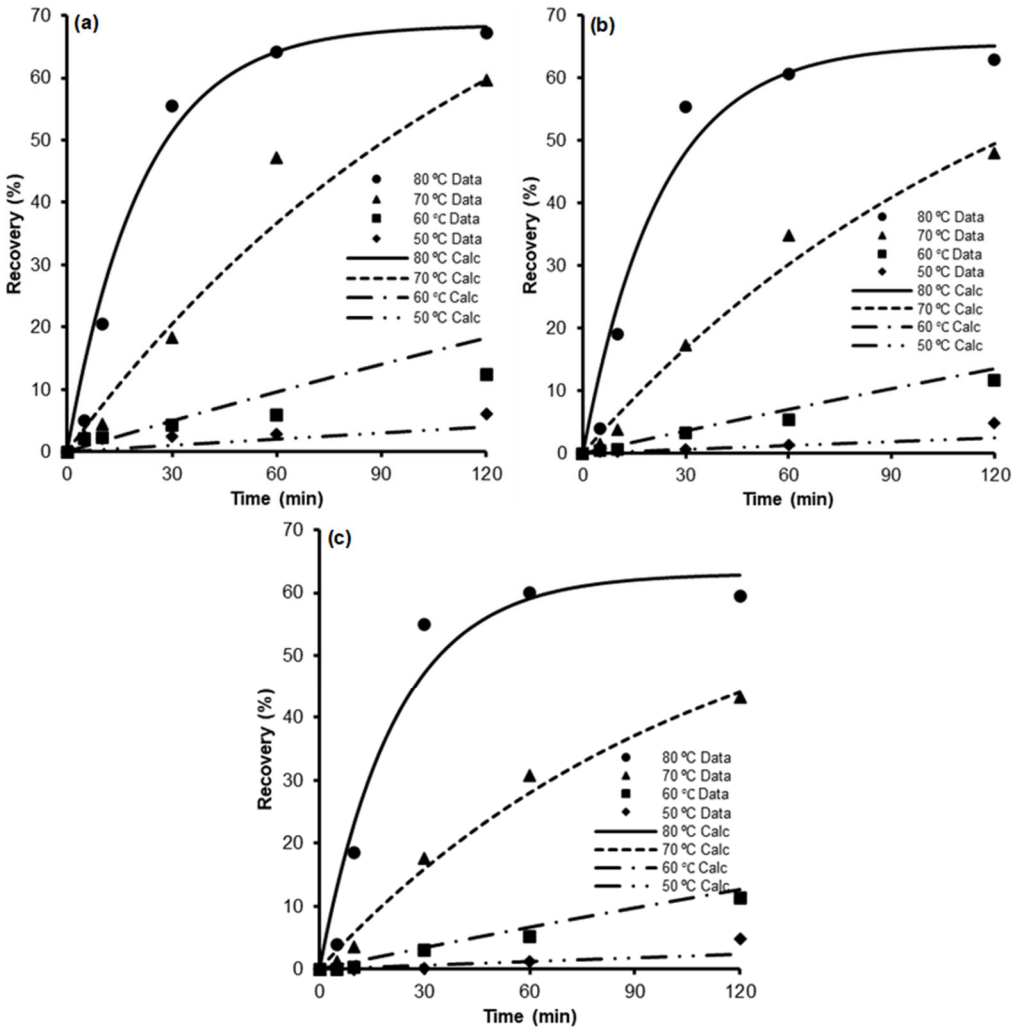

Fig 6. Experimental data and simulation recovery of (a) Li, (b) Ni, and (c) Co

in approaching experimental data is also confirmed by the narrow confidence interval of the fitted parameters.

As depicted in Fig. 6, the calculation results show that a temperature increase leads to a faster recovery rate. Since the rate of forward and backward reactions is both activated by temperature, the maximum recovery of each metal that can be achieved at equilibrium is also determined by temperature. As seen in Fig. 6, the Li recovery tends to be higher at the same temperature than the other metals. Table 2 shows that the activation energies of forward reactions of the metals are relatively similar. Meanwhile, the activation energies of backward reactions decrease significantly for Li, Ni, and Co, in that order. The reaction rate with a higher activation energy would be slower than the others, but the reaction is more sensitive to a temperature change. If the forward reaction is relatively faster than the backward reaction, a higher metal recovery can be expected at equilibrium. For this reason, as seen in Fig. 6, Li could reach its highest recovery faster than the others. It would take a longer time for the other reactions to reach their maximum recovery.

As seen in Table 2, lithium's equilibrium constant (K) decreases as temperature rises. Therefore, the highest Li recovery can be expected at low temperatures. As also shown in Table 2, the activation energy for the backward reactions decreases significantly in the order of Li, Ni, and Co. Therefore, the backward reaction for Li is more sensitive to temperature and thus faster at elevated

Table 2. Kinetics parameters for LMR-NMC cathode leaching with ammonia

Elements	A_f (K^2/min)	A_b (min^{-1})	E_{a_f} (J/mol)	E_{a_b} (J/mol)	T (°C)
Li	$(4.9836\pm0.6299)\times10^{19}$	$(8.2166\pm2.8528)\times10^{71}$	$(1.4331\pm0.0036)\times10^{5}$	$(5.3307\pm0.0041)\times10^{5}$	50 60 70 80
Ni	$(2.4117\pm0.2900)\times10^{21}$	$(5.0455\pm1.5003)\times10^{29}$	$(1.5494\pm0.0034)\times10^{5}$	$(2.4753\pm0.0093)\times10^{5}$	50 60 70 80
Co	$(5.6291\pm0.7953)\times10^{21}$	$(1.6931\pm0.5413)\times10^{17}$	$(1.5743\pm0.0040)\times10^{5}$	$(1.6289\pm0.0092)\times10^{5}$	50 60 70 80

Elements	k_f (min^{-1})	k_b (min^{-1})	K	SSE	R^2
Li	3.4049×10^{-4}	5.8079×10^{-10}	5.8626×10^{5}	0.0320	0.9504
	1.6883×10^{-3}	2.3823×10^{-7}	7.0869×10^{3}		
	7.6256×10^{-3}	6.8935×10^{-5}	1.1062×10^{2}		
	3.1623×10^{-2}	1.4494×10^{-2}	2.1817×10^{0}		
Ni	2.1703×10^{-4}	5.1242×10^{-6}	4.2353×10^{1}	0.0202	0.9640
	1.2255×10^{-3}	8.6521×10^{-5}	1.4164×10^{1}		
	6.2557×10^{-3}	1.2412×10^{-3}	5.0401×10^{0}		
	2.9117×10^{-2}	1.5338×10^{-2}	1.8984×10^{0}		
Co	2.0036×10^{-4}	8.2556×10^{-5}	2.4270×10^{0}	0.0204	0.9616
	1.1633×10^{-3}	5.4147×10^{-4}	2.1484×10^{0}		
	6.0961×10^{-3}	3.1883×10^{-3}	1.9120×10^{0}		
	2.9085×10^{-2}	1.7008×10^{-2}	1.7101×10^{0}		

* $m_f = 2$ and $m_b = 0$

temperatures. Consequently, Li recovery reaches equilibrium faster, whereas Ni and Co require a longer leaching period to achieve maximum recovery.

Thermodynamics Parameters

Table 2 shows the values of the equilibrium constant (K) for each metal determined using Eq. (25). With the use of thermodynamic correlations, it is then possible to calculate the thermodynamic parameters i.e., enthalpy, entropy, and Gibbs free energy. Linearized correlations (Eq. (28)) for each metal are depicted in Fig. 7. As shown in Fig. 7, each correlation line is very close to the experimental data. The thermodynamic parameters obtained from the correlations are presented in Table 3. The correlation lines have a relatively high level of confidence indicated by the R^2 value very close to 1, as shown in Fig. 7.

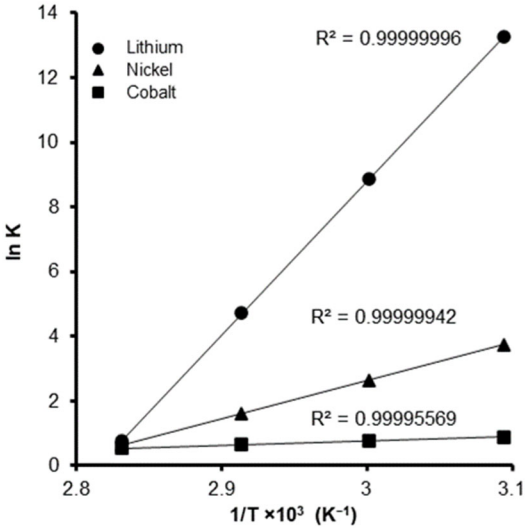

Fig 7. Equilibrium constant as a function of temperature for (a) Li, (b) Ni, and (c) Co

Table 3. Thermodynamics parameters in LMR-NMC cathode leaching with ammonia

Elements	T (°C)	K	ΔH^0 (J/mol)	ΔS^0 (J/mol K)	ΔG^0 (J/mol)
Li	50	5.8626×10^5	-3.9538×10^5	-1.1131×10^3	-3.5683×10^4
	60	7.0869×10^3			-2.4557×10^4
	70	1.1062×10^2			-1.3426×10^4
	80	2.1817×10^0			-2.2905×10^3
Ni	50	4.2353×10^1	-9.8204×10^4	-2.7274×10^2	-1.0064×10^4
	60	1.4164×10^1			-7.3419×10^3
	70	5.0401×10^0			-4.6144×10^3
	80	1.8984×10^0			-1.8821×10^3
Co	50	2.4270×10^0	-1.1075×10^4	-2.6893×10^1	-2.3822×10^3
	60	2.1484×10^0			-2.1181×10^3
	70	1.9120×10^0			-1.8491×10^3
	80	1.7101×10^0			-1.5754×10^3

Table 3 shows that the equilibrium constant for Li, Ni, and Co recoveries decreases with temperature rise. This indicates that a decrease in temperature will shift the reaction towards the formation of reaction product, thereby increasing the maximum recovery achievable at equilibrium. The decrease in the equilibrium constant with temperature rise is associated with the negative values of standard reaction enthalpy and entropy. This means that the reaction is exothermic, indicating that the recovery at equilibrium decreases with an increase in temperature. The Gibbs free energy values for leaching Li, Ni, and Co are negative, suggesting that the leaching process can take place spontaneously. However, an increase in temperature might cause the Gibbs free energy values to become less negative, which suggests that the process becomes less spontaneous. Meanwhile, the standard entropy value of the leaching process is also negative, meaning that the leaching process for Li, Ni, and Co involves the formation of more complicated substances with a lower degree of freedom. The leaching process causes Ni and Co, originally bound in the cathode structure, to become complex ions that have smaller degree of freedom to move. Although Li in the leaching solution is present in its ionic form, the leaching mechanism seems to be dependent on the release of the other metals from the cathode materials.

■ CONCLUSION

Ammonia leaching was able to recover Li, Ni, and Co metals from the NMC-LMR cathodes, while selectively retaining Mn in the residue. In the leaching solution, lithium was present as Li^+ ions while Ni and Co were as complex ions of $Ni(NH_3)_6^{2+}$ and $Co(NH_3)^{2+}$. Mn was precipitated in the residue in the form of $Mn(OH)_2$ and $(NH_4)_2Mn(SO_4)_2$. Increasing the concentration of $(NH_4)_2SO_4$ reagent in a range of 1–2 M and the temperature in a range of 50–80 °C could increase the recovery of Li, Ni, and Co metals. A kinetic model based on equilibrium-shrinking core approach, combined with a modified temperature-dependent Arrhenius model, successfully simulates the recovery of metals. The activation energies of the forward reactions for leaching Li, Ni, and Co were $(1.4331\pm0.0036)\times10^5$, $(1.5494\pm0.0034)\times10^5$, and $(1.5743\pm0.0040)\times10^5$ J/mol, respectively. Meanwhile, the activation energies of the backward reactions for leaching Li, Ni, and Co were $(5.3307\pm0.0041)\times10^5$, $(2.4753\pm0.0093)\times10^5$, and $(1.6289\pm0.0092)\times10^5$ J/mol, respectively. The standard enthalpies for leaching Li, Ni, and Co from NMC-LMR cathodes using ammonia were -3.9538×10^5, -9.8204×10^4, and -1.1075×10^4 J/mol, respectively, while the standard entropies for Li, Ni, and Co were -1.1131×10^3, -2.7274×10^2, and -2.6893×10^1 J/mol K.

The reaction mechanism allowed the leaching recovery of Li, Ni, and Co to increase at low temperatures.

■ ACKNOWLEDGMENTS

The authors are grateful for the financial support provided by The Indonesia Endowment Funds for Education (LPDP) with the Number of Research: PRJ-77/LPDP/2020 through the research project on lithium recovery from spent batteries. The authors also highly appreciate PT. VIAR Indonesia is responsible for supplying spent batteries in this work.

■ CONFLICT OF INTEREST

The authors declare no competing financial interest.

■ AUTHOR CONTRIBUTIONS

Indra Perdana: conceptualization, writing-original draft, writing-review, editing, and visualization. Muhammad Irfan Rahman: conceptualization, methodology, validation, and data curation. Doni Riski Aprilianto: conceptualization, data curation, writing-original draft, writing-review, editing, and visualization. Himawan Tri Bayu Murti Petrus: conceptualization, writing-review, editing, and visualization. Divita Hayyu Kinanti: writing-review, editing, and visualization.

■ REFERENCES

[1] da Silva Lima, L., Quartier, M., Buchmayr, A., Sanjuan-Delmás, D., Laget, H., Corbisier, D., Mertens, J., and Dewulf, J., 2021, Life cycle assessment of lithium-ion batteries and vanadium redox flow batteries-based renewable energy storage systems, *Sustainable Energy Technol. Assess.*, 46, 101286.

[2] Yoshio, M., Brodd, R.J., and Kozawa, A., 2009, *Lithium-Ion Batteries: Science and Technologies*, Springer, New York, US.

[3] Yu, D., Huang, Z., Makuza, B., Guo, X., and Tian, Q., 2021, Pretreatment options for the recycling of spent lithium-ion batteries: A comprehensive review, *Miner. Eng.*, 173, 107218.

[4] Zhang, W., Xu, C., He, W., Li, G., and Huang, J., 2018, A review on management of spent lithium ion batteries and strategy for resource recycling of all components from them, *Waste Manage. Res.*, 36 (2), 99–112.

[5] Zeng, X., Li, J., and Ren, Y., 2012, Prediction of various discarded lithium batteries in China, *2012 IEEE International Symposium on Sustainable Systems and Technology (ISSST)*, Boston, MA, US, 16-18 May 2012.

[6] Kang, D.H.P., Chen, M., and Ogunseitan, O.A., 2013, Potential environmental and human health impacts of rechargeable lithium batteries in electronic waste, *Environ. Sci. Technol.*, 47 (10), 5495–5503.

[7] Zheng, X., Zhu, Z., Lin, X., Zhang, Y., He, Y., Cao, H., and Sun, Z., 2018, A mini-review on metal recycling from spent lithium ion batteries, *Engineering*, 4 (3), 361–370.

[8] Baum, Z.J., Bird, R.E., Yu, X., and Ma, J., 2022, Lithium-ion battery recycling—Overview of techniques and trends, *ACS Energy Lett.*, 7 (2), 712–719.

[9] Islam, M.T., and Iyer-Raniga, U., 2022, Lithium-ion battery recycling in the circular economy: A review, *Recycling*, 7 (3), 33.

[10] Anonymous, 2019, Recycle spent batteries, *Nat. Energy*, 4 (4), 253–253.

[11] Jin, S., Mu, D., Lu, Z., Li, R., Liu, Z., Wang, Y., Tian, S., and Dai, C., 2022, A comprehensive review on the recycling of spent lithium-ion batteries: Urgent status and technology advances, *J. Cleaner Prod.*, 340, 130535.

[12] Free, M.L., 2022, *Hydrometallurgy: Fundamentals and Applications*, Springer, Cham, Switzerland.

[13] Guimarães, L.F., Botelho Junior, A.B., and Espinosa, D.C.R., 2022, Sulfuric acid leaching of metals from waste Li-ion batteries without using reducing agent, *Miner. Eng.*, 183, 107597.

[14] Chen, W.S., and Ho, H.J., 2018, Recovery of valuable metals from lithium-ion batteries NMC cathode waste materials by hydrometallurgical methods, *Metals*, 8 (5), 321.

[15] Xuan, W., de Souza Braga, A., Korbel, C., and Chagnes, A., 2021, New insights in the leaching kinetics of cathodic materials in acidic chloride

media for lithium-ion battery recycling, *Hydrometallurgy*, 204, 105705.

[16] Xuan, W., Otsuki, A., and Chagnes, A., 2019, Investigation of the leaching mechanism of NMC 811 ($LiNi_{0.8}Mn_{0.1}Co_{0.1}O_2$) by hydrochloric acid for recycling lithium ion battery cathodes, *RSC Adv.*, 9 (66), 38612–38618.

[17] Peng, C., Liu, F., Wang, Z., Wilson, B.P., and Lundström, M., 2019, Selective extraction of lithium (Li) and preparation of battery grade lithium carbonate (Li_2CO_3) from spent Li-ion batteries in nitrate system, *J. Power Sources*, 415, 179–188.

[18] Zhuang, L., Sun, C., Zhou, T., Li, H., and Dai, A., 2019, Recovery of valuable metals from $LiNi_{0.5}Co_{0.2}Mn_{0.3}O_2$ cathode materials of spent Li-ion batteries using mild mixed acid as leachant, *Waste Manage.*, 85, 175–185.

[19] Zheng, X., Gao, W., Zhang, X., He, M., Lin, X., Cao, H., Zhang, Y., and Sun, Z., 2017, Spent lithium-ion battery recycling – Reductive ammonia leaching of metals from cathode scrap by sodium sulphite, *Waste Manage.*, 60, 680–688.

[20] Ku, H., Jung, Y., Jo, M., Park, S., Kim, S., Yang, D., Rhee, K., An, E.M., Sohn, J., and Kwon, K., 2016, Recycling of spent lithium-ion battery cathode materials by ammoniacal leaching, *J. Hazard. Mater.*, 313, 138–146.

[21] Liu, X., Huang, K., Xiong, H., and Dong, H., 2023, Ammoniacal leaching process for the selective recovery of value metals from waste lithium-ion batteries, *Environ. Technol.*, 44 (2), 211–225.

[22] Meng, K., Cao, Y., Zhang, B., Ou, X., Li, D., Zhang, J., and Ji, X., 2019, Comparison of the ammoniacal leaching behavior of layered $LiNi_xCo_yMn_{1-x-y}O_2$ (x = 1/3, 0.5, 0.8) cathode materials, *ACS Sustainable Chem. Eng.*, 7 (8), 7750–7759.

[23] Ning, P., Meng, Q., Dong, P., Duan, J., Xu, M., Lin, Y., and Zhang, Y., 2020, Recycling of cathode material from spent lithium ion batteries using an ultrasound-assisted DL-malic acid leaching system, *Waste Manage.*, 103, 52–60.

[24] Munir, H., Srivastava, R.R., Kim, H., Ilyas, S., Khosa, M.K., and Yameen, B., 2020, Leaching of exhausted LNCM cathode batteries in ascorbic acid lixiviant: A green recycling approach, reaction kinetics and process mechanism, *J. Chem. Technol. Biotechnol.*, 95 (8), 2286–2294.

[25] Li, L., Lu, J., Ren, Y., Zhang, X.X., Chen, R.J., Wu, F., and Amine, K., 2012, Ascorbic-acid-assisted recovery of cobalt and lithium from spent Li-ion batteries, *J. Power Sources*, 218, 21–27.

[26] Refly, S., Floweri, O., Mayangsari, T.R., Aimon, A.H., and Iskandar, F., 2021, Green recycle processing of cathode active material from $LiNi_{1/3}Co_{1/3}Mn_{1/3}O_2$ (NCM 111) battery waste through citric acid leaching and oxalate co-precipitation process, *Mater. Today: Proc.*, 44, 3378–3380.

[27] Mishra, D., Kim, D.J., Ralph, D.E., Ahn, J.G., and Rhee, Y.H., 2008, Bioleaching of metals from spent lithium ion secondary batteries using *Acidithiobacillus ferrooxidans*, *Waste Manage.*, 28 (2), 333–338.

[28] Huang, T., Liu, L., and Zhang, S., 2019, Recovery of cobalt, lithium, and manganese from the cathode active materials of spent lithium-ion batteries in a bio-electro-hydrometallurgical process, *Hydrometallurgy*, 188, 101–111.

[29] Moosakazemi, F., Ghassa, S., Jafari, M., and Chelgani, S.C., 2023, Bioleaching for recovery of metals from spent batteries – A review, *Miner. Process. Extr. Metall. Rev.*, 44 (7), 511–521.

[30] Mustika, P.C.B.W., Suryanaga, E.C., Perdana, I., Sutijan, S., Astuti, W., Petrus, H.T.B.M., and Prasetya, A., 2023, Optimization of lithium separation from NCA leachate solution: Investigating the impact of feed concentration, pressure, and complexing agent concentration, *ASEAN J. Chem. Eng.*, 23 (3), 343–359.

[31] Nitta, N., Wu, F., Lee, J.T., and Yushin, G., 2015, Li-ion battery materials: Present and future, *Mater. Today*, 18 (5), 252–264.

[32] Houache, M.S.E., Yim, C.H., Karkar, Z., and Abu-Lebdeh, Y., 2022, On the current and future outlook of battery chemistries for electric vehicles—Mini review, *Batteries*, 8 (7), 70.

[33] Schmuch, R., Wagner, R., Hörpel, G., Placke, T., and Winter, M., 2018, Performance and cost of

materials for lithium-based rechargeable automotive batteries, *Nat. Energy*, 3 (4), 267–278.

[34] Smith, A.J., Smith, S.R., Byrne, T., Burns, J.C., and Dahn, J.R., 2012, Synergies in blended $LiMn_2O_4$ and $Li[Ni_{1/3}Co_{1/3}Mn_{1/3}]O_2$ positive electrodes, *J. Electrochem. Soc.*, 159 (10), A1696.

[35] Meng, F., Liu, Q., Kim, R., Wang, J., Liu, G., and Ghahreman, A., 2020, Selective recovery of valuable metals from industrial waste lithium-ion batteries using citric acid under reductive conditions: Leaching optimization and kinetic analysis, *Hydrometallurgy*, 191, 105160.

[36] Refly, S., Floweri, O., Mayangsari, T.R., Sumboja, A., Santosa, S.P., Ogi, T., and Iskandar, F., 2020, Regeneration of $LiNi_{1/3}Co_{1/3}Mn_{1/3}O_2$ cathode active materials from end-of-life lithium-ion batteries through ascorbic acid leaching and oxalic acid coprecipitation processes, *ACS Sustainable Chem. Eng.*, 8 (43), 16104–16114.

[37] Gao, W., Song, J., Cao, H., Lin, X., Zhang, X., Zheng, X., Zhang, Y., and Sun, Z., 2018, Selective recovery of valuable metals from spent lithium-ion batteries – Process development and kinetics evaluation, *J. Cleaner Prod.*, 178, 833–845.

[38] Liu, B., Huang, J., Song, J., Liao, K., Si, J., Wen, B., Zhou, M., Cheng, Y., Gao, J., and Xia, Y., 2022, Direct recycling of spent $LiNi_{0.5}Co_{0.2}Mn_{0.3}O_2$ cathodes based on single oxalic acid leaching and regeneration under mild conditions assisted by lithium acetate, *Energy Fuels*, 36 (12), 6552–6559.

[39] Semenov, N.N., 1958, *Some Problems of Chemical Kinetics and Reactivity*, Pergamon Press, London, UK.

[40] Setiawan, H., Petrus, H.T.B.M., and Perdana, I., 2019, Reaction kinetics modeling for lithium and cobalt recovery from spent lithium-ion batteries using acetic acid, *Int. J. Miner. Metall. Mater.*, 26 (1), 98–107.

[41] Kohout, J., 2021, Modified Arrhenius equation in materials science, chemistry and biology, *Molecules*, 26 (23), 7162.

[42] Smith, I.W.M., 2008, The temperature-dependence of elementary reaction rates: Beyond Arrhenius, *Chem. Soc. Rev.*, 37 (4), 812–826.

[43] Julien, C.M., and Massot, M., 2003, Lattice vibrations of materials for lithium rechargeable batteries I. Lithium manganese oxide spinel, *Mater. Sci. Eng., B*, 97 (3), 217–230.

[44] Lin, Y., Zhao, S., Qian, J., Xu, N., Liu, X.Q., Sun, L.B., Li, W., Chen, Z., and Wu, Z., 2020, Petal cell-derived MnO nanoparticle-incorporated biocarbon composite and its enhanced lithium storage performance, *J. Mater. Sci.*, 55 (5), 2139–2154.

[45] Essehli, R., Sabri, S., El-Mellouhi, F., Aïssa, B., Ben Yahia, H., Altamash, T., Khraisheh, M., Amhamed, A., and El Bali, B., 2020, Single crystal structure, vibrational spectroscopy, gas sorption and antimicrobial properties of a new inorganic acidic diphosphates material $(NH_4)_2Mg(H_2P_2O_7)_2{\cdot}2H_2O$, *Sci. Rep.*, 10 (1), 8909.

[46] Zheng, R., Wang, W., Dai, Y., Ma, Q., Liu, Y., Mu, D., Li, R., Ren, J., and Dai, C., 2017, A closed-loop process for recycling $LiNi_xCo_yMn_{1-x-y}O_2$ from mixed cathode materials of lithium-ion batteries, *Green Energy Environ.*, 2 (1), 42–50.

[47] Di Vincenzo, A., and Floriano, M.A., 2020, Elucidating the influence of the activation energy on reaction rates by simulations based on a simple particle model, *J. Chem. Educ.*, 97 (10), 3630–3637.

[48] Laurendeau, N.M., 2005, *Statistical Thermodynamics: Fundamentals and Applications*, Cambridge University Press, Cambridge, UK.

[49] Lafuente, B., Downs, R.T., Yang, H., and Stone, N., 2015, "The Power of Databases: The RRUFF Project" in *Highlights in Mineralogical Crystallography*, Eds. Armbruster, T., and Danisi, R.M., De Gruyter, Berlin, Germany.